Chinese Chemical Letters 35 (2024) 109080

Contents lists available at ScienceDirect

Chinese Chemical Letters

journal homepage: www.elsevier.com/locate/cclet

Deciphering the high-carbonization-temperature triggered enzymatic activity of wool-derived N, S-co-doped carbon nanosheets

Jiachen Zhao[a,1], Deshuai Yu[a,1], Jianmin Chen[b,d,*], Shihao Lin[c], Yonghua Tang[a], Chaoyu Fan[a], Dongfang Zhou[c,*], Youhui Lin[a,*]

[a] Department of Physics, Research Institute for Biomimetics and Soft Matter, Fujian Provincial Key Laboratory for Soft Functional Materials Research, Xiamen University, Xiamen 361005, China
[b] School of Pharmacy and Medical Technology, Putian University, Putian 351100, China
[c] Key Laboratory of Mental Health of the Ministry of Education, NMPA Key Laboratory for Research and Evaluation of Drug Metabolism & Guangdong Provincial Key Laboratory of New Drug Screening, School of Pharmaceutical Sciences, Southern Medical University, Guangzhou 510515, China
[d] Key Laboratory of Pharmaceutical Analysis and Laboratory Medicine (Putian University), Fujian Province University, Putian 351100, China

ARTICLE INFO

Article history:
Received 25 June 2023
Revised 8 September 2023
Accepted 9 September 2023
Available online 15 September 2023

Keywords:
Carbon-based nanozyme
Catalytic mechanism
Density functional theory
High-temperature carbonization

ABSTRACT

It is well-established that high carbonization temperature will trigger the enzyme-like activity of carbon-based materials. However, the catalytic mechanism is still ambiguous, which hinders the further rational design of nanomaterials as enzyme mimics. Hereby, N, S-rich carbonized wool nanosheets (CWs) were synthesized at different pyrolysis temperatures. As expected, only CWs treated with high-temperature possess intrinsic oxidase- and peroxidase-like activities. Meanwhile, density functional theory (DFT) calculations demonstrate that graphitic nitrogen and the co-existence of nitrogen and sulfur in the carbon matrix serve as the active sites for the enzyme-like process. More importantly, combining theoretical calculations and experimental observations, the high-temperature triggered catalytic mechanism can be ascribed to the fact that an appropriate high-temperature maximizes the graphitization degree to a certain extent, at which most of the catalytic active sites are well retained rather than evaporating. Moreover, coupling with excellent photothermal conversion efficiency and catalytic performance, CWs can be applied to photothermal-catalytic cancer therapy under near-infrared region (NIR) light irradiation. We believe this work will contribute to understanding the catalytic mechanism of carbon-based nanozymes and promote the development of new biomedical and pharmaceutical applications.

© 2023 Published by Elsevier B.V. on behalf of Chinese Chemical Society and Institute of Materia Medica, Chinese Academy of Medical Sciences.

Nanozymes, nanomaterials that possess intrinsic enzyme-like characteristics, were proposed since the Fe_3O_4 nanoparticles were first discovered to exhibit peroxidase-like activity in 2007 [1]. Although most of them cannot match the catalytic performance of natural enzymes, they take advantage of excellent stability, low cost, and ease of synthesis [2]. Up to now, tremendous efforts have been made to develop nanozymes, and various nanozymes have been driven from noble metals, metal oxides, metal-organic frameworks, and carbon-based materials [3–6]. Among them, carbon-based nanozymes, including graphene oxide, carbon dot, carbon nanotube, and various carbon nanomaterials carbonized from different precursors, have received huge attention due to their unique physiochemical properties, high performance, and tunable activities [7–11]. In particular, it is known that high carbonization temperature would trigger the enzyme-like activity of carbon precursor. However, the catalytic mechanism is still ambiguous due to the complex factors involved. Previous studies have demonstrated that the sufficient graphitization degree brought by high carbonization temperatures is essential for the catalytic process in carbon-based materials, while the inevitable evaporation of heteroatoms is out of consideration [12,13]. It is recognized that heteroatoms in the carbon matrix are crucial for enzyme-like activity and may serve as the active sites for the catalytic process [14,15]. Therefore, it is urgent to elucidate the detailed mechanism of the enzyme-like activity in nonmetal carbon-based materials triggered by high-temperature carbonization.

Wool, a natural biopolymer with excellent biocompatibility, is one of the most promising and abundant protein sources. The main component of wool is keratin, the hierarchical structure composed of a variety of α-amino acid residues with a high concentration of cysteine [16]. Therefore, the chemical nature makes it

* Corresponding authors.
E-mail addresses: chenjianmin1985@sina.com (J. Chen), dfzhou@smu.edu.cn (D. Zhou), linyouhui@xmu.edu.cn (Y. Lin).
[1] These authors contributed equally to this work.

https://doi.org/10.1016/j.cclet.2023.109080
1001-8417/© 2023 Published by Elsevier B.V. on behalf of Chinese Chemical Society and Institute of Materia Medica, Chinese Academy of Medical Sciences.

could be converted into the heteroatoms (*e.g.*, nitrogen and sulfur) abundant carbonized wool nanosheets *via* simple pyrolysis without complex chemical processes. Moreover, previous works have demonstrated that introducing the second heteroatom (*e.g.*, sulfur, boron, and phosphorus) could enhance the enzyme-like activity of N-doped carbon materials [12,17,18]. In addition, previous studies using biomaterials to construct heteroatom-abundant carbon materials are excellent in catalytic activity [19-21]. Therefore, the wool was chosen as the carbon precursor to investigate the detailed mechanism of the high-temperature triggered enzyme-like activity by controlled regulation of the chemical compositions and structures at different carbonization temperatures. Meanwhile, compared with traditional nonmetal carbon-based materials, CWs feature ultra-low cost, ease of fabrication, and environmental benignity. In addition, other unique properties of carbon-based nanomaterials, such as photothermal conversion ability, were not taken seriously in most catalytic systems. Thus, enzyme-like characteristics of nanozymes and their physiochemical properties as nanomaterials should be fully considered.

In this work, it is demonstrated that N, S-rich carbonized wool nanosheets could serve as efficient oxidase and peroxidase mimics only at high carbonization temperatures. The experimental characterization indicates the increasing graphitization degree and carbon defect amounts of CWs as the rising of carbonization temperatures, with the relatively stable content of graphitic N, sulfur, and oxygen-functional groups and dramatically decreased pyridinic N and pyrrolic N amounts. Meanwhile, we performed DFT calculations to identify the catalytic active sites responsible for the enzyme-like activities. The calculation results demonstrate the graphitic N and the co-existence of N and S serve as the active center to activate the nearby carbon to mimic peroxidase, while the S itself near N is active for the oxidase-like activity. Moreover, we use graphene as the carbon precursor to construct N-, O-, and S-doped graphene, and their enzyme-like activity is consistent with our DFT calculation results. Therefore, combining both theoretical calculations and experimental observation, the intrinsic catalytic mechanism could be ascribed to the high graphitization degree of CWs at the balanced carbonization temperature, at which most catalytic active sites are well retained instead of evaporation (Scheme 1). Moreover, the as-prepared CWs exhibit high photothermal performance under the NIR light. By combining both excellent photothermal properties and catalytic performance, CWs could be used for photothermal-enhanced tumor catalytic treatment. We expect this work may help to accelerate the understanding of the detailed catalytic mechanism of nanozymes and explore new applications of CWs.

Herein, N, S-rich CWs were synthesized through simple one-step carbonization using wool as the protein precursor (Scheme 1). Typically, wool carbonized at 900 °C under the nitrogen atmosphere with a ramp rate of 2 °C/min was grounded and donated as CW-900. Transmission electron microscopy (TEM) and scanning electron microscopy (SEM) were performed to investigate the size and morphology of the CW-900. The CW-900 presents graphene-like nanosheet morphology, and the size of the synthesized sample was a few micrometers (Fig. 1a and Fig. S1 in Supporting information). In order to investigate the structural changes after the carbonization, the X-ray powder diffractometer (XRD) and Fourier transform infrared spectroscopy (FTIR) were used to examine the structures of wool and CW-900. The XRD pattern of the wool showed a broad peak at about 22.4°. In comparison, two new peaks emerged in the XRD pattern after carbonization at 900 °C (Fig. 1b). The diffraction peak at ~25° was ascribed to the (002) plane of graphite, which indicates the formation of the hexagonal conjugated carbon matrix (Fig. 1b) [8]. Meanwhile, another peak located at ~43.5° was donated as the lattice plane (100) of disordered graphite [22]. Besides, comparing the FTIR

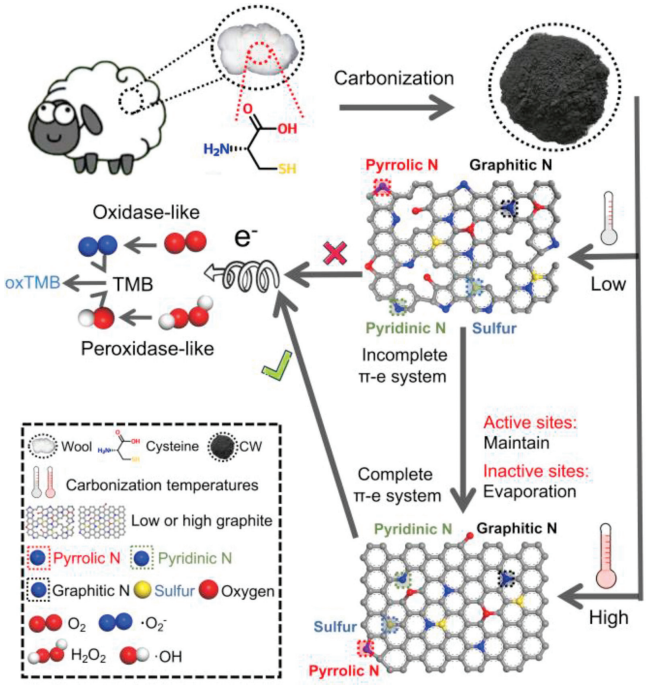

Scheme 1. Schematic illustration of procedures for the preparation of N, S-rich carbonized wool nanosheets and the corresponding high-temperature triggered catalytic mechanism.

micro-spectra of CWs and wool, the emergence of C–N peak (1105 cm^{-1}), and the disappearance of the amide peak (amide I at 1660 cm^{-1}, amide II at 1538 cm^{-1}, and amide III at 1244 cm^{-1}) indicated the replacement of amide structures by hexagonal conjugated carbon structures due to high-temperature carbonization (Fig. S2a in Supporting information) [23]. Meanwhile, with the rising carbonization temperatures, the C–N peak becomes sharper, indicating the formation of nanosheet structures of CW-900. As mentioned above, it is expected the chemical nature of wool could make CW-900 rich in N and S elements. Therefore, X-ray photoelectron spectroscopy (XPS) was used to examine the surface chemical compositions of the CW-900. As depicted in Fig. 1c, the survey spectra demonstrated the presence of carbon, oxygen, nitrogen, and sulfur elements on the surface of CW-900, per our expectations. Furthermore, four types of nitrogen were found in the high-resolution N 1s XPS spectrum, which is assigned as pyridinic N (398.47 eV), pyrrolic N (399.88 eV), graphitic N (400.82 eV), and oxidized N (402.7 eV), respectively (Fig. 1d) [14]. Meanwhile, the high-resolution S 2p spectrum exhibits three peaks associated with C−S−C (163.9 eV for S $2p_{3/2}$, 165.2 eV for S $2p_{1/2}$) and C−SO_x−C (168.3 eV) species, which indicates the S atom was inlaid in the carbon matrix (Fig. 1e) [24]. Moreover, the high-resolution C 1s XPS spectrum also confirms the existence of heteroatoms N and O (Fig. 1f) [22]. Also, the high-resolution O 1s XPS spectrum confirms the main oxygen-functional groups of CW-900 are the hydroxyl and carboxyl groups (Fig. S2b in Supporting information). In addition, SEM-energy dispersive X-ray spectroscopy (EDS) was also used to examine the elemental composition of CW-900. As shown in Fig. 1g, the full coverage of carbon, oxygen, nitrogen, and sulfur elements are uniformly dispersed on CW-900, which is consistent with the XPS results. Therefore, the above results demonstrated the N, S-co-doped carbon nanosheet was successfully synthesized.

Due to the abundant N and S elements in the carbon matrix, it is expected that CW-900 would possess intrinsic enzyme-like activity. Herein, the enzyme-like activity of CW-900 was investigated using 3,3′,5,5′-tetramethylbenzidine (TMB) as the typical

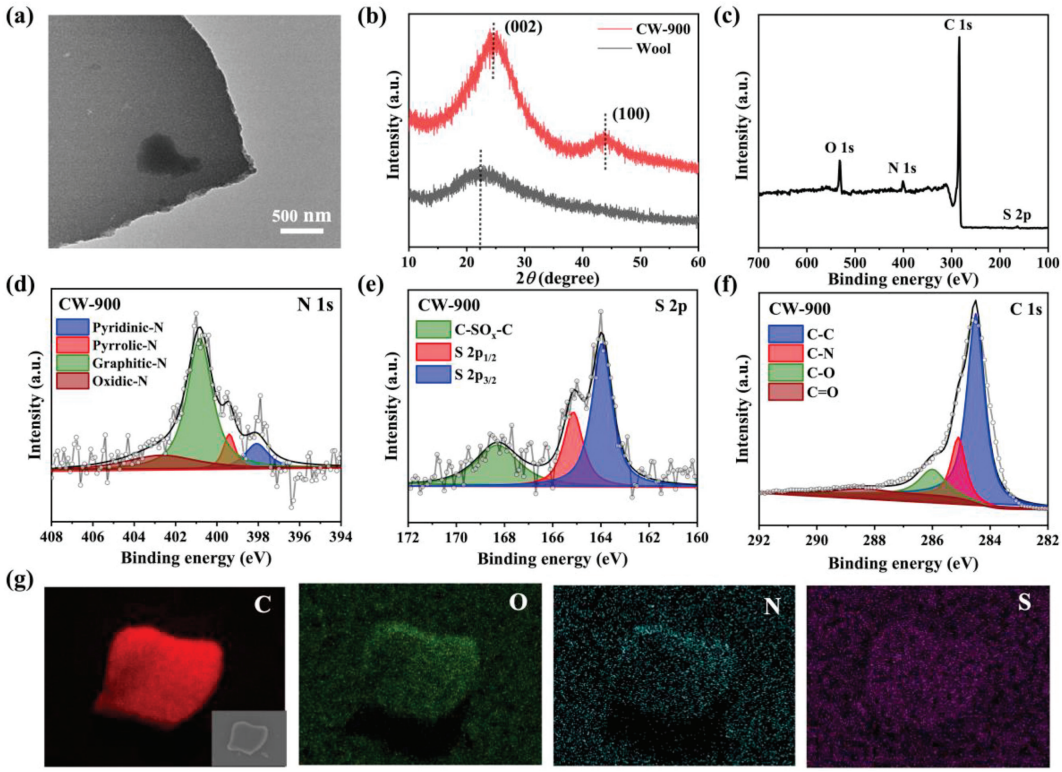

Fig. 1. Structure characterization of CW-900. (a) TEM image. (b) XRD patterns. (c) XPS survey spectra. (d) High-resolution N 1s XPS spectra. (e) High-resolution S 2p XPS spectra. (f) High-resolution C 1s XPS spectra. (g) SEM image and corresponding EDS mappings.

probe molecule due to the oxidation of TMB could be determined by monitoring the change in absorbance of the reaction solution [25]. Meanwhile, we also checked the water dispersity of CW-900, and the result indicates they were well dispersed in water (Fig. S3 in Supporting information). As depicted in Fig. 2a, oxidase-like activity refers to the ability to oxidase substrate with oxygen molecules [26]. According to Fig. 2b, the absorbance spectrum of the reaction solution holds pronounced absorption peaks at around 652 nm in the presence of CW-900, while no peak was found in pure TMB solution. The absorption peaks located at around 652 nm could be attributed to the oxidation of TMB to oxTMB, which indicates the CW-900 could serve as the oxidase mimic. To further verify that CW-900 could act as the oxidase mimic, we choose other substrates (3-ethylbenzothiazoline-6-sulfonic acid diammonium salt (ABTS) and O-phenylenediamine (OPD)) to evaluate their oxidase-like activity. The results show the ABTS could be oxidized into the green color product $ABTS^{+}$, while the OPD could be oxidized into the yellow color product by CW-900 (Fig. S4 in Supporting information) [25]. Meanwhile, the influence of pH and temperature of the CW-900 as the oxidase mimic was also evaluated, with the optimal oxidase-like activity at pH 3 (Fig. S5b in Supporting information). Moreover, CW-900 possesses better oxidase-like activity at a high reaction temperature (50 °C) (Fig. S5a in Supporting information). Furthermore, to verify the Michaelis-Menten kinetics of CW-900 as the oxidase mimic, the reaction rates at different TMB concentrations were measured (Figs. 2c and d). The higher maximum reaction rate (v_{max}) value of CW-900 than other carbon-based nanozymes indicated excellent oxidase-like activity (Table S1 in Supporting information). In addition, it is believed that the oxidase-like activity of nanozymes may be ascribed to the oxygen molecules dissolved in water that could be transformed by nanozymes into a superoxidase radical anion ($^{\bullet}O_2^-$) to oxidized substrate [27,28]. Hereby, we performed electron spin resonance (ESR) to detect the reactive intermediates during the enzyme-like reaction. Using 5-*tert*-butoxycarbonyl5-methyl-1-pyrroline *N*-oxide (BMPO) as a probe, the typical signals of BMPO/$^{\bullet}O_2^-$ were distinctly seen in the ESR spectrum (Fig. 2e).

After successfully verifying the oxidase-like activity of CW-900, the peroxidase-like activity was also systematically studied. As shown in Fig. 2a, peroxidase-like activity refers to the ability to oxidase substrate with the presence of hydrogen peroxide [29]. Similarly, the absorption peaks located at around 652 nm were stronger in the presence of CW-900, indicating that CW-900 exhibits intrinsic peroxidase-like activity (Fig. 2f). Meanwhile, the ABTS and OPD were also used as probe molecules to verify the peroxidase-like activity of CW-900. The results are consistent when using TMB (Fig. S4 in Supporting information). Similar to the oxidase-like activity of CW-900, the peroxidase-like activity was also dependent on pH and temperature (Fig. S6 in Supporting information). The optimal condition for peroxidase-like activity of CW-900 was determined to be pH 3 and 40 °C. Furthermore, the kinetic parameters of CW-900 were obtained using H_2O_2 as the substrate (Figs. 2g and h). Our CW-900 exhibits better binding affinity toward H_2O_2 than most carbon-based nanozymes, and even the natural horseradish peroxidase (HPR) (Table S2 in Supporting information) [30]. Meanwhile, the catalytic constants (v_{max}) of CW-900 for peroxidase-like activity were higher than part of previously reported carbon-based nanomaterials (Table S2). In addition, four signature peaks with a relative 1:2:2:1 intensity ratio appeared in the ESR spectra of the BMPO/H_2O_2/CW-900 system verifying the formation of $^{\bullet}OH$, which was deemed to be the origin of peroxidase-like activity of nanozymes (Fig. 2i).

In order to reveal the catalytic mechanism of the high-temperature triggered enzyme-like activity of CW-900, a series of carbonized samples by varying the carbonization temperature from 400 °C to 900 °C was synthesized to investigate the influence of the composition and structures on the enzyme-like activity. As expected, the catalytic activity of CWs is enhanced along

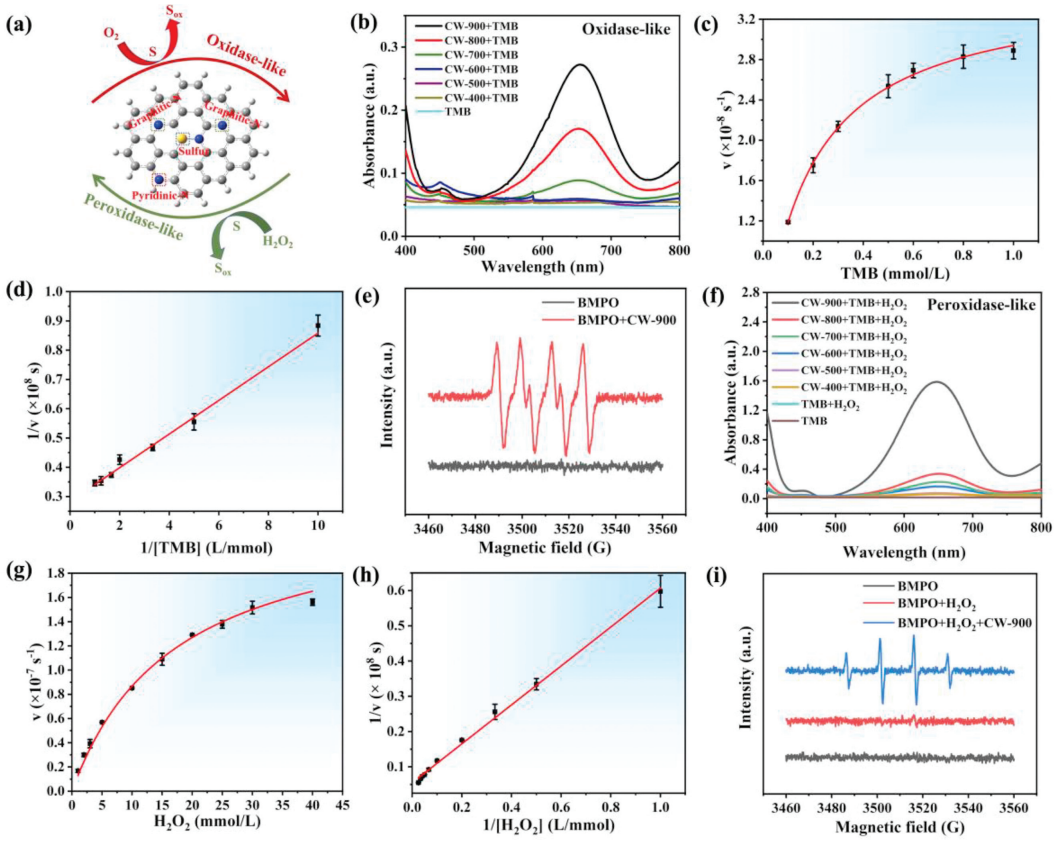

Fig. 2. Oxidase- and peroxidase-like activity of CWs. (a) Schematic illustration of the oxidase- and peroxidase-like process. (b) UV–vis curves of TMB solutions with CWs. (c, d) Kinetics for oxidase-like activity of CW-900. (e) ESR spectra of BMPO, and BMPO + CW-900. (f) UV–vis curves of TMB solutions with CWs and H_2O_2. (g, h) Kinetics for peroxidase-like activity of CW-900. (i) ESR spectra of BMPO, BMPO + H_2O_2, and BMPO + H_2O_2 + CW-900.

with the carbonization temperatures increasing (Figs. 2b, 2f, and 3a). Therefore, XRD was used to investigate the effect of different carbonization temperatures on their structures. As shown in Fig. S7 (Supporting information), the (100) lattice plane in the XRD pattern of CWs started to appear at the carbonization temperatures rise to 700 °C, which indicates the emergence of disordered carbon. Meanwhile, the intensity ratio of the D and G bands (I_D/I_G) in Raman spectroscopy demonstrated the defect carbon content is higher with the increase of pyrolysis temperatures (Table S3 in Supporting information) [31]. The disordered carbon ring in the carbon matrix could change the electron structure of the π-electron system and was reported to promote the catalytic performance of carbon-based materials [32,33]. Besides, the Raman spectroscopy showed gradually narrowed D and G bands of the CWs along the increased carbonization temperatures, indicating a more stable graphite structure was formed (Fig. S8 in Supporting information) [22]. Furthermore, by analyzing the high-resolution C 1s XPS spectrum of CWs, the C–C content increased with the carbonization temperatures, which means a higher degree of graphitization (Fig. S9 in Supporting information). The higher graphitization degree suggests a larger π-electron system that could promote electron transfer and stabilize intermediates, which is essential for the catalytic possess [8]. As depicted in Fig. S10 (Supporting information), both oxidase- and peroxidase-like activity of CWs appears at the graphitization degrees reaches about 55%, and increases along with the graphitization degrees. Moreover, the enzyme-like activity of CWs rapidly increases as the graphitization degrees reach almost 65%, which indicates that a sufficient graphitization degree of carbon-based materials is necessary for the catalytic process. In addition, previous studies also indicate that heteroatom doping could enhance the catalytic of carbon-based nanozymes. However, the atomic content of N in CWs decreases significantly with the increase of pyrolysis temperatures, while the atomic content of S is rather stable (Table S4 in Supporting information). After analyzing the high-resolution N 1s XPS spectrum of CWs, we found as the increasing pyrolysis temperatures, the relative content of graphitic N increased while the pyridinic N and pyrrolic N reduced (Figs. S11 and S12 in Supporting information). This phenomenon resulted in a relatively stable absolute content of graphitic N and dramatically decreased amounts of pyridinic N and pyrrolic N in CWs as the rise of the temperatures (Fig. 3b). This is quite understandable, given the graphitic N linked with three carbon atoms in the carbon matrix should be more stable than pyridinic N and pyrrolic N which linked with two carbon atoms in the edge. Meanwhile, besides heteroatoms, the amounts of oxygen-functional groups in CWs are stable and may influence their enzyme-like activity (Table S4).

Based on the above discussion, we performed DFT calculations to investigate the detailed catalytic mechanism at the atomic level. Different graphene models containing nitrogen, sulfur, nitrogen-sulfur, and oxygen-functional groups were constructed [17] (Fig. S13 in Supporting information). Then, to investigate the origin of the peroxidase-like activity of CW-900, the DFT calculations on the peroxidase-like catalytic process under acidic conditions were conducted. In order to determine the catalytic active site, several potential active sites were chosen, including the S atom, N atom, C atom near the S/N atom, and C atom near oxygen-functional groups. Gibbs free energy diagrams and intermediate conformations of the peroxidase-mediated reactions were constructed for several sites (Fig. 3c and Figs. S14–S26 in Supporting information). Meanwhile, the energy barrier of the rate-determining step (RDS) for the peroxidase-like reaction is given in Fig. 3d. As depicted in

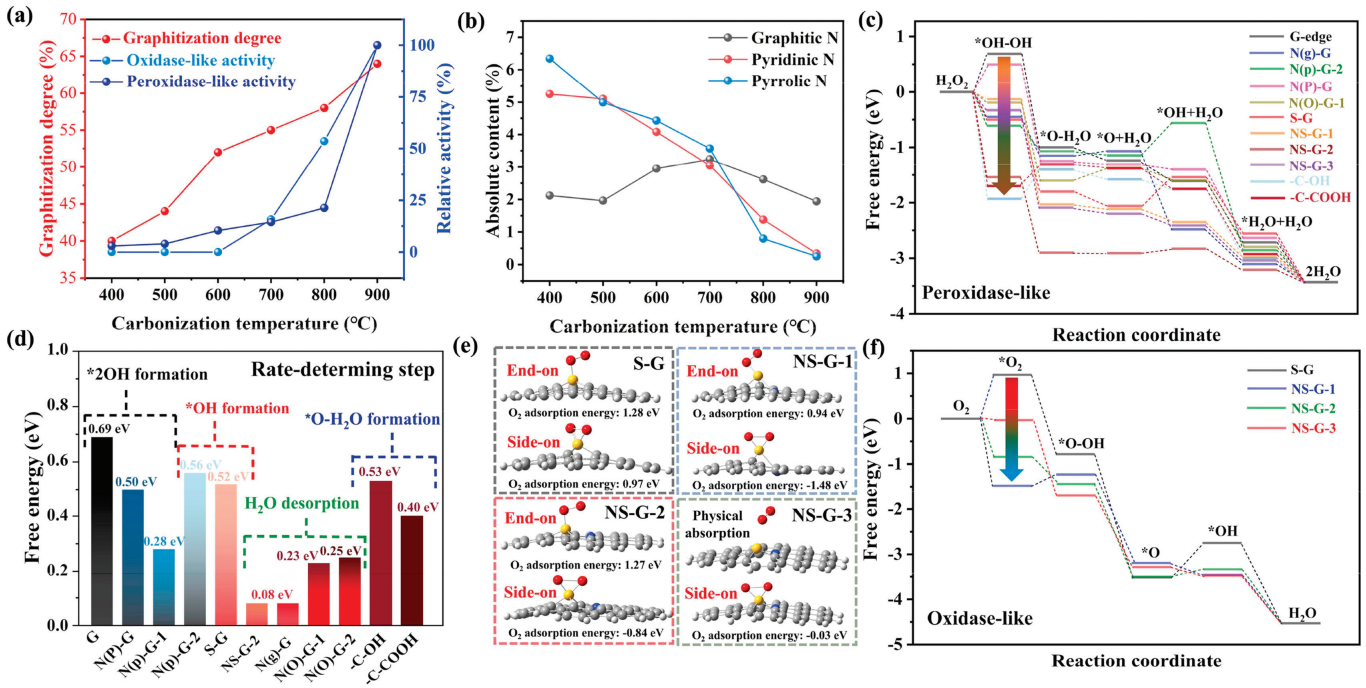

Fig. 3. Intrinsic catalytic mechanism of CWs as peroxidase and oxidase mimic. (a) Change of catalytic activities and graphitization degree of CWs along carbonization temperature varying. (b) Absolute atomic content of graphitic, pyridinic, and pyrrolic N in CWs treated with different temperatures. (c) Gibbs free energy diagram of peroxidase-like reaction in chosen models. (d) The energy barriers of the rate-determining step (RDS) in the chosen models as peroxidase mimic. (e) $^*O_2$ adsorption configuration and corresponding adsorption energy. (f) Gibbs free energy diagram of oxidase-like reaction in chosen models.

Fig. S14, the Gibbs free energy diagram of graphene without any doping showed that the C atoms on the basal plane and edge have a high energy barrier for *2OH formation and therefore are catalytically inert.

After introducing the N atom to the carbon matrix, the RDS energy barriers of peroxidase-like reaction were reduced compared to pure graphene, because they could activate the nearby C atom to act as active sites (Fig. 3d and Figs. S15–S20). Meanwhile, among different N forms, graphitic N in the carbon matrix is most active for the peroxidase-like reaction, with tiny RDS energy barriers of 0.08 eV, followed by oxidized N, pyridinic N, and pyrrolic N (Fig. 3d). In addition, the RDS energy barriers of graphitic N-doped graphene is much lower than other forms of N-doped graphene, which indicates the graphitic N is the main active site for the peroxidase-like reaction among all forms of N species (Fig. 3d). Next, the effect of S in the carbon matrix on the peroxidase-like activity is also evaluated. We found that both the C atom near the S atom and the S atom itself could act as active sites (Fig. S21 in Supporting information). Although the formation of *2OH on S-G model is thermodynamically favorable, the *OH adsorption energy is relatively high and leads to a non-negligible RDS energy barrier (0.52 eV) for *OH formation (Fig. 3d). Intriguingly, in the case of N, S-co-doping, the peroxidase-like reaction process holds negligible energy barriers, which is beneficial for the reaction evolution (Fig. 3d and Figs. S22–S24). In addition, we also evaluate whether the oxygen-functional groups influence the peroxidase-like activity of CW-900. The results indicate that both C–OH and C–COOH could promote the peroxidase-like reaction compared to pure graphene (Fig. 3d and Figs. S25 and S26). However, the relatively high RDS energy barriers of oxygen-functional group modified graphene compared to graphitic N-doped or N, S-co-doped graphene indicates they are not the main active sites for the peroxidase-like reaction in CW-900 (Fig. 3d). Therefore, the graphitic N and the N, S-co-doping are the major active sites for the peroxidase-like reaction in CW-900 predicted by DFT calculations.

Next, DFT calculations on the oxidase-like catalytic process under acidic conditions were also performed using the same models. Our calculation results indicate that only the sulfur atom in the carbon matrix could adsorb and activate the O_2 molecule. Meanwhile, we also investigated the two typical O_2 adsorption configurations (end-on and side-on models) on the chosen models. The results indicate that O_2 prefers the side-on adsorption configuration on the S atom in the carbon matrix (Fig. 3e). Gibbs free energy diagrams and intermediate conformations of the oxidase-mediated reactions are shown in Fig. 3f and Fig. S27 (Supporting information). As depicted in Fig. 3f, the O_2 adsorption in S-G is thermodynamic prohibition, with a huge energy barrier of 0.97 eV, while is thermodynamically favorable in NS-G. To further investigate the reason that the S atom near N is more active than the S atom alone, we performed charge difference density and Hirshfeld atomic charge calculations. It is obvious that the charge transfer exists between the S atom and the N atom (Fig. S28 in Supporting information). Compared to the S atom in S-G, the N atom near the S atom in NS-G would transfer electrons to the S atom, making the S atom more active for O_2 absorption (Table S5 in Supporting information). Meanwhile, tiny thermodynamic energy barriers exist in N, S-co-doped graphene (0.26 eV for NS-G-1, 0.18 eV for NS-G-2, and 0.0 eV for NS-G-3), which indicates that sulfur near nitrogen atom in the carbon matrix is responsible for the intrinsic oxidase-like activity of CW-900 (Fig. 3f).

To further verify the results of our theoretical calculations, we use graphene to construct N-, S-, and O-doped graphene, referred to as N-G, S-G, and O-G. TEM images reveal the graphene-sheet morphology of N-G, S-G, and O-G (Fig. S29 in Supporting information). Meanwhile, the XPS survey spectra demonstrated the presence of C, O, and N atoms on the surface of N-G, C, O, and S atoms on the surface of S-G, and only C and O atoms in O-G (Fig. S30a in Supporting information). Moreover, the high-resolution N 1s XPS spectrum indicates the presence of pyridinic N, pyrrolic N, graphitic N, and oxidized N on the surface of N-G (Fig. S30c in Supporting information). Also, the high-resolution O 1s XPS spec-

trum indicates the presence of C–OH and C–COOH in O-G, and the O atom content in O-G (10.42%) is much higher than in N-G (2.93%) (Fig. S30d and Table S6 in Supporting information). The high-resolution S 2p spectrum of S-G exhibits two peaks associated with C–S–C (163.9 eV for S $2p_{3/2}$, 165.2 eV for S $2p_{1/2}$) species (Fig. S30e in Supporting information). As a result, the peroxidase-like activity of O-G and S-G is much lower than N-G, indicating that the oxygen-functional groups or S atom itself as active sites are much inferior to the N atom, consistent with our DFT calculations (Fig. S31c in Supporting information). Meanwhile, the oxidase-like activity is highest in N-G, followed by O-G and S-G (Fig. S31d in Supporting information). However, the oxidase-like activity of N-G is much lower than CW-900, demonstrating that only N, S-co-doping could act as active sites for the oxidase-like activity (Fig. S31b in Supporting information).

Therefore, although the low-carbonization temperature-treated CWs are rich in catalytically active sites, the incomplete π-electron system resulting from the low graphitization degree is unable to accelerate electron transfer to stabilize the intermediates, which leads to negligible enzyme-like activity (Scheme 1). As the rise of the pyrolysis temperature, the graphitization of CWs increases with the sharply decreased content of heteroatom N (from 13.73% in CW-400 to 3.18% in CW-900), while the amount of graphitic N and sulfur as the catalytic sites remain stable (Fig. 3b). Moreover, the emergence of oxidized N in CW could also act as the active site for peroxidase-like reaction. The above discussion could be ascribed to the origin of the excellent enzyme-like activity of CW-900. Thus, an appropriate carbonization temperature that could balance the graphitization degree and the catalytic site amounts is crucial to the catalytic performance of carbon-based nanomaterials. Moreover, whether the degree of graphitization or the number of catalytic active sites has more influence on the catalytic activity of carbon-based materials is crucial for the rational design of high-performance carbon catalysts. As mentioned above, we use pristine graphene to synthesize highly graphitized N-G. As a result, the N-G possesses a higher graphitization degree than CW-900 (Figs. S9 and S30b in Supporting information). Meanwhile, the N-G has much less graphitized N content (0.62%) than CW-900 (1.92%) as active sites for peroxidase-like activity (Fig. S30c and Table S6). Moreover, there are no S atoms on the surface of N-G (Table S6). However, the peroxidase-like activity of N-G is still higher than CW-900, which indicates the graphitization degree may be a more important factor for the catalytic activity of carbon-based materials (Fig. S31a in Supporting information).

Furthermore, to investigate whether increasing the carbonization temperature would further increase the enzyme-like activity of CW, we increased the carbonization temperatures to 1200 °C. The results indicate the N atom amounts decreased from 3.18% in CW-900 to 1.62% in CW-1200, while the O atom amounts sharply increased from 6.88% in CW-900 to 15.61% in CW-1200 (Table S4). Meanwhile, both peroxidase- and oxidase-like activity of CW-1200 is much lower than CW-900 (Fig. S32 in Supporting information). The decrease of enzyme-like activity in CW-1200 could be attributed to the ultra-high carbonization temperature leading to the evaporation of both heteroatoms and carbon atoms, destroying the carbon skeleton and leading to the low graphitization degree of CW-1200 (Fig. S32 in Supporting information). The low graphitization degree of CW-1200 leads to a decrease in its reactivity. Therefore, we believe that with a further increase in the carbonization temperature, the enzyme-like activity of CW would increase to an extreme value and then decrease. Combining both theoretical calculations and experimental observations, the high-temperature triggered catalytic mechanism can be attributed to appropriate high-temperature maximizes the graphitization degree to a certain extent, at which most of the catalytic active sites are well retained rather than evaporating (Figs. 3a and b and Table S4).

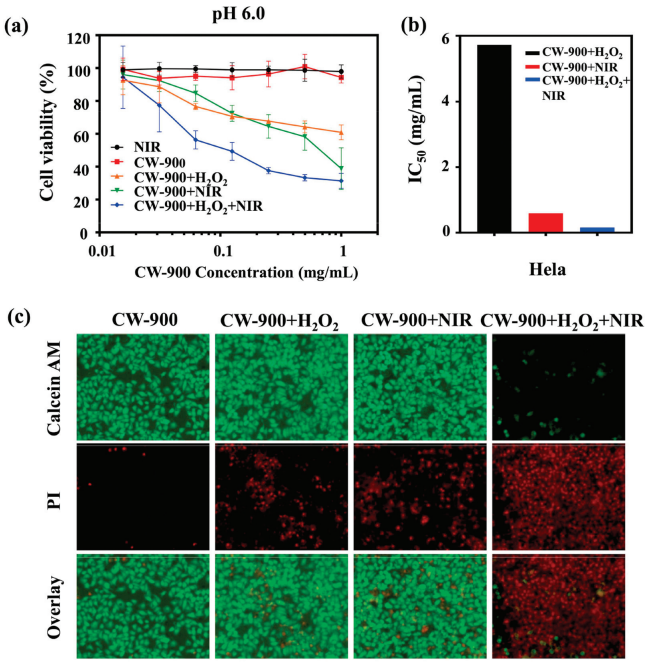

Fig. 4. *In vitro* tumor therapeutic. (a) Cell viabilities of HeLa cells (DMEM, pH 6.0) treated by NIR, CW-900, CW-900 + H_2O_2 (75 μmol/L), CW-900 + NIR and CW-900 + H_2O_2 + NIR. All the above groups were irradiated by an 808 nm laser (0.8 W/cm^2, 3 min). (b) IC_{50} of Hela cells treated with CW-900 + H_2O_2, CW-900 + NIR and CW-900 + H_2O_2 + NIR. (c) Fluorescence microscopy images of Calcein AM and PI contained HeLa cells after various treatments indicated (CW-900: 1 mg/mL; 808 nm laser: 0.8 W/cm^2, 5 min). Green and red colors represented live and dead cells, respectively.

It is well-established that carbon-based materials possess unique physiochemical characteristics besides catalytic activity, such as photothermal conversion ability. Typically, photothermal conversion refers to the ability that can convert the absorbed photons into heat, thereby raising the local temperature [34]. In this work, an 808 nm NIR light source was used to study the photothermal conversion efficiency of CW-900, due to the NIR light features handiness, deeper penetration, and minimal unwanted effects on human tissue than visible light [35]. As shown in Fig. S33a (Supporting information), the solution containing CW-900 significantly enhances the photothermal conversion performance compared to the control medium. The temperature of the solution containing CW-900 increased from 22.5 °C to 52 °C after 5 min of NIR light irradiation, whereas the temperature of the control media was almost unchanged (Fig. S33c in Supporting information). In addition, the temperature is also dependent on the NIR power density, which increases with the power density (Fig. S33b in Supporting information).

It has been shown previously that the production of reactive oxygen species (ROS) from nanozymes can efficiently kill cancer cells [36]. Meanwhile, carbon-based nanomaterials can also act as a photothermal agent for tumor treatment [37]. Therefore, we expect CW-900 could be used as a photothermal-catalytic agent for cancer therapy. To evaluate the feasibility and efficacy of CW-900 for tumor catalytic therapy, the human cervical carcinoma cell line HeLa was used. Since the CW-900 exhibits optimal peroxidase-like activity under acidic conditions, the photodynamic therapy efficiency of CW-900 was measured by incubating with Hela cells in DMEM media, pH 6.0. Cell viability analysis showed that the combination treatment of H_2O_2, NIR, and CW-900 decreased HeLa cell viability with an IC_{50} of 0.1566 mg/mL, which is more than 30-fold lower than that of the CW-900 + H_2O_2 group and more than 3-fold lower than that of the CW-900 + NIR group (Figs. 4a and b). However, NIR or CW-900 only had no effect on HeLa

cells viability under the same conditions (Fig. 4a). It is known that cancer cells inside solid tumors are able to constitutively produce H_2O_2 (from $\sim 5.0 \times 10^{-5}$ mol/L to 1.0×10^{-4} mol/L) [38]. Therefore, 7.5×10^{-5} mol/L of H_2O_2 was added to mimic the tumor microenvironment. Compared to CW-900 alone in the dark, or under NIR alone, the combined treatment by CW-900 offered the most effective cancer cell killing, which could be further enhanced with additional H_2O_2 added (Fig. 4a). This data was also consistent with our results using live/death staining assay (Fig. 4c). More importantly, cell death was most pronounced in the CW-900 + H_2O_2 + NIR group, verifying that hydrogen peroxide can be catalyzed by CW-900 into ROS and enhance the killing effect of photothermal therapy on tumor cells.

In summary, the N, S-rich carbon-based nanozymes with intrinsic oxidase- and peroxidase-like activity were successfully synthesized using wool as the precursor *via* a facile, economical, and effective method. Meanwhile, the catalytic active sites of CW for the enzyme-like activity were determined using both DFT calculations and experiments, in which the graphitic N and the co-existence of N and S atoms serve as the active center to activate the nearby carbon to mimic peroxidase, while the S atom itself near N is responsible for the oxidase-like activity. More importantly, combining both theoretical calculation and experimental results, the high-temperature triggered enzyme-like activity could be attributed to an appropriate high-temperature that maximizes the graphitization degree to a certain extent, at which most of the catalytic active sites are well retained instead of evaporating. In addition, we found that the graphitization degree is a more important factor for the catalytic activity of carbon-base materials than the active site amounts. Thus, a desired carbonization temperature that could balance the graphitization degree and catalytic site amounts is crucial to the catalytic performance of carbon-based nanomaterials. Moreover, due to the ability to generate ROS and heat, CW can act as a robust agent for synergistic photothermal-catalytic tumor therapy. Our acquired results shed light on the catalytic mechanism of non-metal carbon-based material as nanozyme and pave the way to use wool for further developing carbon-based nanozymes.

Declaration of competing interest

The authors declare that they have no known competing financial interests or personal relationships that could have appeared to influence the work reported in this paper.

Acknowledgments

This research was funded by the National Natural Science Foundation of China (Nos. 12274356, 22275081), Key Laboratory of Pharmaceutical Analysis and Laboratory Medicine (Putian University) (No. PALM 202206), Fujian Province University, the Fundamental Research Funds for the Central Universities (No. 20720220022), and the 111 Project (No. B16029). The authors also thank Prof. Zhisen Zhang, Dr. Yun Yang, and Hao Wang for valuable discussions and technical assistance.

Supplementary materials

Supplementary material associated with this article can be found, in the online version, at doi:10.1016/j.cclet.2023.109080.

References

[1] H. Wei, E. Wang, Anal. Chem. 80 (2008) 2250–2254.
[2] D. Jiang, D. Ni, Z.T. Rosenkrans, et al., Chem. Soc. Rev. 48 (2019) 3683–3704.
[3] Y. Sun, B. Xu, X. Pan, et al., Coord. Chem. Rev. 475 (2023) 214896.
[4] L. Zheng, F. Wang, C. Jiang, et al., Coord. Chem. Rev. 471 (2022) 214760.
[5] Q. Liu, A. Zhang, R. Wang, Q. Zhang, D. Cui, Nano-Micro Lett. 13 (2021) 154.
[6] W. Chen, S. Li, J. Wang, K. Sun, Y. Si, Nanoscale 11 (2019) 15783–15793.
[7] H. Sun, A. Zhao, N. Gao, et al., Angew. Chem. Int. Ed. 54 (2015) 7176–7180.
[8] W. Gao, J. He, L. Chen, et al., Nat. Commun. 14 (2023) 160.
[9] Y. Song, K. Qu, C. Zhao, J. Ren, X. Qu, Adv. Mater. 22 (2010) 2206–2210.
[10] S. Lin, Y. Zhang, W. Cao, et al., Dalton Trans. 48 (2019) 1993–1999.
[11] H. Wang, P. Li, D. Yu, et al., Nano Lett. 18 (2018) 3344–3351.
[12] Q. Liang, J. Xi, X.J. Gao, et al., Nano Today 35 (2020) 100935.
[13] Z. Wu, Y. Lv, Y. Xia, P.A. Webley, D. Zhao, J. Am. Chem. Soc. 134 (2012) 2236–2245.
[14] Y.H. Hu, X.J.J. Gao, Y.Y. Zhu, et al., Chem. Mater. 30 (2018) 6431–6439.
[15] H.B. Wang, M.L. Zhang, K.Q. Wei, et al., Carbon 179 (2021) 692–700.
[16] B. Wang, W. Yang, J. McKittrick, M.A. Meyers, Prog. Mater. Sci. 76 (2016) 229–318.
[17] M.S. Kim, S. Cho, S.H. Joo, et al., ACS Nano 13 (2019) 4312–4321.
[18] S. Luo, M. Sha, F. Tian, et al., Chin. Chem. Lett. 33 (2022) 344–348.
[19] M. Xia, X. Zhang, Z. Xie, ACS Sustain. Chem. Eng. 10 (2022) 14330–14342.
[20] Y. Hou, M. Xia, Y. Han, et al., J. Colloid Interface Sci. 638 (2023) 291–299.
[21] M. Xia, S. Li, Z. Xie, Chem. Commun. 59 (2023) 2783–2786.
[22] X.Q. Xiong, Y.H. Tang, C.J. Xu, et al., Small 16 (2020) 2004129.
[23] S. Ling, Z. Qi, D.P. Knight, Z. Shao, X. Chen, Biomacromolecules 12 (2011) 3344–3349.
[24] Y. Wang, L. Yu, W. Zhu, et al., Ionics 25 (2019) 3499–3522.
[25] B. Jiang, D. Duan, L. Gao, et al., Nat. Protoc. 13 (2018) 1506–1520.
[26] X. Shen, W. Liu, X. Gao, et al., J. Am. Chem. Soc. 137 (2015) 15882–15891.
[27] H. Wei, E. Wang, Chem. Soc. Rev. 42 (2013) 6060–6093.
[28] J. Wu, X. Wang, Q. Wang, et al., Chem. Soc. Rev. 48 (2019) 1004–1076.
[29] Y. Jiang, J. Zhu, L. Li, et al., Nanoscale 14 (2022) 7596–7606.
[30] T. Lin, L. Zhong, L. Guo, F. Fu, G. Chen, Nanoscale 6 (2014) 11856–11862.
[31] Y. Jia, L. Zhang, A. Du, et al., Adv. Mater. 28 (2016) 9532–9538.
[32] X. Wang, Y. Jia, X. Mao, et al., Chem 6 (2020) 2009–2023.
[33] G. Ye, S. Liu, K. Zhao, Z. He, Angew. Chem. Int. Ed. 62 (2023) e20230340.
[34] C. Xu, C. Zhao, M. Li, et al., Small 10 (2014) 1841–1847.
[35] H. Wang, J. Di, Y. Sun, et al., Adv. Funct. Mater. 25 (2015) 5537–5547.
[36] Y. Dai, Y. Ding, L. Li, Chin. Chem. Lett. 32 (2021) 2715–2728.
[37] Y. Yang, D. Zhu, Y. Liu, et al., Nanoscale 12 (2020) 13548–13557.
[38] T.P. Szatrowski, C.F. Nathan, Cancer Res. 51 (1991) 794–798.